Gallego-Sánchez, EM.; Li, C.; Paris, C.; Martín-García, N.; Martínez-Triguero, J.; Boronat Zaragoza, M.; Moliner Marin, M.... (01-1). Making Nanosized CHA Zeolites with Controlled Al Distribution for Optimizing Methanol-to-Olefin Performance. Chemistry - A European Journal. 24(55):14631-14635. https://doi.org/10.1002/chem.201803637

Improving the MTO performance by optimizing the Al distribution within nanosized CHA-type catalysts

Eva M. Gallego,[+] Chengeng Li,[+] Cecilia Paris, Nuria Martín, Joaquín Martínez-Triguero, Mercedes Boronat, Manuel Moliner,* Avelino Corma*

Instituto de Tecnología Química, Universitat Politècnica de València-Consejo Superior de Investigaciones Científicas, Avenida de los Naranjos s/n, 46022 València, Spain

*Corresponding authors: E-mail addresses: acorma@itq.upv.es; mmoliner@itq.upv.es

[+] These authors have contributed equally

The methanol to olefins (MTO) process allows the efficient generation of light olefins, such as ethylene or propylene, which are considered platform molecules to obtain several main compounds for the petrochemical industry.[1] Small pore zeolites containing large cavities within their structure have been recognized as active and highly stable catalysts for the MTO process.[2] The presence of the large cavities favors the formation and stabilization of the aromatic polymethylbenzene intermediates according to the accepted "hydrocarbon pool" (HP) mechanism,[3] while the small pores allow the diffusion of the linear light olefins, particularly ethylene and propylene, that are generated by successive methylation and cracking of the HP intermediates (see Figure 1).[4] Nevertheless, these light olefins may further react yielding longer chain hydrocarbons, or participate in the aging of the aromatic HP intermediates into other polyaromatic species, like naphthalenes or phenanthrenes, that hinder the diffusion of products and finally block the cavities, leading to catalyst deactivation.[4b, 5]

Up to now, the silicoaluminophosphate (SAPO) form of the CHA structure, named SAPO-34,[6] is the preferred catalyst for the MTO process,[7] because it exhibits a low tendency to deactivate by excessive formation of bulky aromatic products, especially when tested at moderate-high reaction temperatures (i.e. 450-500°C).[4a] However, its aluminosilicate counterpart, SSZ-13, presents a higher intrinsic activity and a lower optimum reaction temperature (i.e. 350-375°C),[5b] which makes it a promising alternative to SAPO-34 as catalyst for the MTO process. In order to enhance the catalytic performance of the aluminosilicate SSZ-13, particularly its stability against deactivation, many recent research efforts have focused on decreasing the diffusion pathways of reactants and products within the SSZ-13 particles, including the preparation of nanosized crystals,[8] or with high intra-crystalline mesoporosity.[9]

A different factor that needs to be considered in relation to catalyst performance is the amount and distribution of Brønsted acid sites within the zeolite framework. According to the hydrocarbon pool mechanism proposed for the MTO reaction, each cavity in the CHA structure can only host one aromatic polymethylbenzene HP species under working conditions, compensated by one framework Al atom (see Figure 2a). Increasing the Si/Al ratio would necessarily result in less cavities able to form the HP species and, therefore, in a lower activity or catalyst life time (see Figures 2b and 2c). Moreover, for a given Al content, placing two Al atoms close to each other in the same cavity results in a decrease in the total number of hydrocarbon pool species present (see Figures 2b and 2d), and might also accelerate undesired oligomerization and condensation reactions leading to blocking of cavities. Therefore, it could be envisioned that, in principle, an optimum catalytic performance should be achieved with a homogeneous distribution of active sites corresponding to one Al center per cavity.

In this sense, it has been described recently that the presence of sodium cations in the synthesis gel plays a fundamental role on the final Al distribution within the crystallized SSZ-13 zeolites, with the amount of Al-pairs, mainly within the 6-rings present in the CHA cavities, increasing with the sodium content.[10] Considering the negative effect of paired Al centers on the MTO activity of SSZ-13 proposed above, it appears that the sodium-free synthesis of the aluminosilicate SSZ-13, particularly within nanosized crystals, should maximize its catalytic performance and lifetime.

Herein, we will present the first synthesis descriptions of sodium-free nanocrystalline SSZ-13 materials with average crystal sizes in the nanoscale values (~60-80 nm) with controlled Si/Al molar ratios (~15 and 25), by combining the use of pre-crystallized FAU zeolites as silicon and aluminum sources with N,N,N,-trimethyladamantammonium ($TMAda^+$) as OSDA. The Na-free nanocrystalline SSZ-13 zeolites perform as excellent catalysts for the MTO reaction and, particularly, the Na-free nanosized SSZ-13 with a Si/Al molar ratio of ~15, shows, at least, a 5-fold increase of the catalyst life compared to the standard SSZ-13 material reported in the literature. The precise effect of sodium cations on the Al-distribution within the CHA-based catalysts has been theoretically proven. The achieved results demonstrate that the combination of the nanocrystalline size with an optimized aluminum distribution within the SSZ-13 zeolite, allows a significant enhancement of its catalytic performance for the MTO reaction.

To understand the influence of sodium on the Al distribution in SSZ-13 zeolite, the relative stability of different structures containing $TMAda^+$, Na^+, or a combination of both as compensating cations, was studied by means of DFT calculations. It was found that, for isolated Al sites, $TMAda^+$ cations always occupy the center of the large CHA cavities and, preferentially, stabilize the Al atoms located close to the methyl groups directly bonded to the cationic N center (see Figure S1a). In contrast, Na^+ cations are preferentially placed in the center of the 6-rings of the small cages, forming three or four strong bonds with the framework O atoms (see Figure S1b). Al pairs, defined as Al atoms in close proximity separated by either one or two Si atoms [Al−O(−Si−O)$_x$−Al; x=1,2], require the presence of two proximal compensating cations. Two $TMAda^+$ will be necessarily placed in two different cavities and, therefore, only some particular arrangements of pairs could be stabilized by these cations. As shown in Figure S1c, structures with two Al atoms in the same 6-ring are, at least, 5 kcal/mol less stable than a distribution with the two Al in different cavities, and Al pairs with only one Si between the two Al atoms are clearly unstable. However, the location of Na^+ in the center of the 6-ring permits the presence of a $TMAda^+$ cation in close proximity (see Figure S1d), allowing the stabilization of structures containing two Al atoms in the same small cage, or in the same 6-ring.

With these trends in mind, we explored a number of Al distributions corresponding to a Si/Al = 11 (that is, three Al per unit cell) using either only $TMAda^+$ or a combination of $TMAda^+$ and Na^+ to compensate the negative charges generated in the framework. As clearly observed in Table S1, the most stable structures using exclusively $TMAda^+$ as compensating cations are those containing just one Al atom per cavity (structures 1-5), as well as structure 6 (see Figure S2), in which one of the two Al atoms belonging to the same 6-ring is stabilized by a $TMAda^+$ cation placed in the neighboring cavity. The rest of distributions considered are between 7 and 22 kcal/mol less stable. In contrast, when one of the three framework Al atoms is compensated by a Na^+ cation placed in the center of the 6-ring, most distributions containing Al pairs are clearly stabilized. Structure 6 (see Figure S2), with two Al atoms in the same 6-ring, becomes the global minimum, and some other distributions with Al pairs (like structures 10 and 11, see Figure S2) compete in stability with the highly dispersed systems (structures 1-3, see Figure S2) obtained in the absence of Na^+. It can then be concluded from the DFT study that the presence of Na^+ cations together with $TMAda^+$ leads to an increase in the concentration of Al pairs in the CHA structure. Therefore, in order to obtain SSZ-13 zeolite with a homogeneous distribution of centers corresponding to one Al atom per cavity, the presence of Na^+ should be avoided in the synthesis.

The standard synthesis of the SSZ-13 zeolite uses amorphous sources of silicon and aluminum, and requires the combination of $TMAda^+$ and Na^+ (see CHA_1 in Table S2 and synthesis details in the Supplementary Material).[11] This standard SSZ-13 material shows an average crystal size of 1-2 µm with a Si/Al molar ratio of ~15 (see CHA_1 in Table 1). To evaluate the effect of sodium, the preparation of the SSZ-13 zeolite has been attempted under similar synthesis conditions, but removing the presence of sodium from the synthesis media. In this sense, two different Si/Al ratios have been proposed, ~15 and ~30 (see CHA_2 and CHA_3, respectively, in Table S2 and synthesis details in the Supplementary Material). The achieved solids show the crystalline structure of CHA (see PXRD patterns of CHA_2 and CHA_3 in Figure S3), and their Si/Al molar ratios are analogous to those introduced initially in the gels (17.4 and 26.7 for CHA-2 and CHA-3, respectively, see Table 1). These sodium-free CHA samples show similar crystal sizes to the standard CHA_1 material, with average sizes of ~ 1 µm (see CHA_2 and CHA_3 in Figure 3).

These materials have been calcined at 580°C to remove the organic species occluded within the crystalline structures, and in the case of the sodium-containing CHA_1 sample, this sample has been ammonium-exchanged to remove the extra-framework sodium cations and, finally, calcined at 500°C to generate its acid-form. After these treatments, the three materials are

essentially free of sodium cations. The coordination of the aluminum atoms in these calcined materials has been studied by solid ^{27}Al MAS NMR spectroscopy (see Figure S4). The solid ^{27}Al MAS NMR spectra of the three SSZ-13 zeolites are similar, presenting a main band centered at ~55 ppm that has been assigned to tetrahedrally coordinated Al atoms in framework positions, and a very small signal at ~0 ppm that has been assigned to octahedrally coordinated Al species in extra-framework positions (see Figure S4). A careful quantification indicates that above 90-95% of the entire Al species remain in framework positions in the three micron-sized SSZ-13 materials.

Recently, Gounder et al. have measured the fraction of Al-pairs within high-silica CHA zeolites by using a Co^{2+}-exchange procedure.[10] Following this titration method, we have observed that the amount of Al-paired species is almost twice for the CHA_1 sample, which has been synthesized with the presence of sodium in the synthesis media, compared to the two sodium-free CHA samples (see Table S3). These experimental results are in good agreement with our theoretical calculations, where the precise role of sodium cations in the synthesis media favoring the formation of Al-pairs along the crystallized CHA zeolites was unraveled.

These SSZ-13 catalysts have been tested for the MTO reaction at WHSV=0.8 h^{-1} and 350°C (see reaction conditions in the Supplementary Material). On the one hand, the standard CHA-1 material shows methanol conversion drops below 95% and 50% after 210 and 316 minutes, whereas CHA_2, which was synthesized under analogous conditions but in absence of sodium cations in the synthesis media, presents improved catalyst lifetimes, requiring 260 and 490 minutes to achieve 95 and 50% methanol conversion drops, respectively (see Table 2 and Figure 4). Since both materials have similar crystal sizes and Si/Al molar ratios (see Table 1), it could be hypothesized that the presence of sodium during the synthesis preparation of the standard CHA_1 zeolite has indeed an influence on the Al distribution along the crystals. In fact, for a given Si/Al molar ratio, the higher is the percentage of Al pairs within the zeolite crystals, the lower is the amount of Al-containing CHA cavities capable of forming the required bulky aromatic MTO intermediate species (see Figures 2b and 2d). On the other hand, the CHA_3 sample, which was synthesized under sodium-free conditions with a Si/Al molar ratio of ~26, presents a remarkably lower catalytic activity than CHA_2, which was also synthesized under Na-free conditions with a Si/Al molar ratio of ~17 (X_{50} ~ 490 and 335 minutes for CHA_2 and CHA_3, respectively, see Table 2). In this case, the less amount of Al-containing CHA-cavities within CHA_3 compared to CHA_2 could explain its limited catalyst behavior. Moreover, it is important to remark that CHA_3 performs with a similar methanol conversion profile compared

to the standard CHA_1 zeolite (X_{50} ~ 320-335 minutes, see Table 2), even when the standard SSZ-13 presents a remarkably lower Si/Al molar ratio (~ 15, see Table 1). These results would also confirm the negative effects of sodium in the synthesis media on homogenously distributing the aluminum atoms as single species within the CHA cavities, and its direct implications on the MTO catalytic performance.

Once the negative influence of the sodium cations on the MTO catalytic activity when CHA-related zeolites are employed as catalysts is established, it would be important to rationalize the preparation of these materials in order to maximize their catalytic behavior. As stated in the introduction, the reduction of the crystal size into the nanometer scale should improve the catalytic performance by enhancing the diffusion pathways of reactants and products. Recently, it has been shown that the use of pre-crystallized FAU-type zeolites as source of Si and Al in the synthesis media, could favor the crystallization of some target zeolites in their nanocrystalline form.[12] According to this, we proposed the sodium-free synthesis of the nanocrystalline SSZ-13 zeolites combining the use of FAU and TMAda as former Si and Al source and OSDA, respectively. For this purpose, two commercially available FAU zeolites (CBV720, Si/Al~14; CBV760, Si/Al~26) have been employed as sole silicon and aluminum precursors for the synthesis of CHA-4 and CHA-5, respectively (see Supplementary Material for synthesis details). The resultant solids show the characteristic PXRD patterns of the CHA structure (see CHA-4 and CHA-5 in Figure S3). Very interestingly, the achieved crystals of CHA-4 and CHA-5 show homogeneous nanocrystallites for both samples, with average sizes of 60 and 80 nm, respectively (see FE-SEM images in Figure 3). The chemical analyses reveal final Si/Al molar ratios of 14.2 and 24.1 for the CHA-4 and CHA-5 samples (see Table 1), which are similar values to those initially introduced in the synthesis gels by the FAU-type precursors.

These Na-free nanocrystalline SSZ-13 materials have been calcined in air at 580°C to remove the organic species, and the calcined samples have been evaluated by ^{27}Al MAS NMR spectroscopy to study the coordination of the aluminum atoms (see Figure S4). In both cases, the solid ^{27}Al MAS NMR spectra indicate that almost 90-95% of the Al species remain in tetrahedral coordination, as revealed by the main band centered at ~55 ppm (see CHA_4 and CHA_5 in Figure S4).

When these two nanocrystalline SSZ-13 samples, CHA_4 and CHA_5, have been tested for the MTO reaction, it is observed that they show much longer catalyst lifetimes than the previously tested micron-sized SSZ-13 zeolites (see Figure 4). It is particularly significant the catalyst lifetime enhancement achieved when using the nanocrystalline CHA_4 material, which shows a five-fold

increase compared to the standard SSZ-13 zeolite (see Figure 4 and Table 2). These results highlight the importance of controlling the crystal size in the nanometric scale to improve the diffusion rate of reactants and products, particularly the diffusion of the produced light olefins, mostly precluding the excessive formation of coke by undesired oligomerization reactions.

At this point, and for comparison results, we have prepared the nanosized CHA-based material described in the literature, named SSZ-62 zeolite.[8a] According to the methodology described by Zones et al.,[8a] this material can be prepared with very small crystal sizes (below 50 nm) and Si/Al molar ratios of ~ 8. The preparation of the SSZ-62 material is favored under highly alkaline synthesis conditions, requiring high sodium hydroxide contents ($NaOH/SiO_2$ ~ 0.4, see Table S2 and experimental details in the Supplementary Material). The PXRD pattern of the as-prepared solid reveals the crystallization of the CHA material as pure phase (see CHA_6 in Figure S3), while the study of the sample by FE-SEM shows the nanocrystalline nature of the sample (~30-40 nm, see CHA_6 in Figure 3). The chemical analysis indicates that the Si/Al molar ratio of the nanosized CHA_6 material is ~8.5, which is lower than the theoretical Si/Al molar ratio introduced initially in the synthesis gel (Si/Al ~15). This fact could be explained by the high alkalinity required for the synthesis of the SSZ-62, forcing to some silicon species to remain as soluble silicates. The as-prepared nanosized CHA_6 material has been calcined at 580°C and NH_4-exchanged to generate its acid-form.

As it could be expected, the nanocrystalline nature of the SSZ-62 material led to an enhancement of the catalyst lifetime compared to the micron-sized standard SSZ-13 zeolite (X_{50} ~ 316 and 514 minutes for the CHA_1 and CHA_6, respectively, see Figure 4 and Table 2). However, the nanosized SSZ-62 (CHA_6) material shows a considerably lower catalytic activity than the other two-nanosized CHA materials synthesized above (see Figure 4). As seen in Table 2, the CHA_4 and CHA_5 materials present a 3- and 2-fold increase of the catalyst lifetime compared to SSZ-62 (X_{50} ~ 1693, 1048 and 514 minutes for CHA_4, CHA_5 and CHA_6, respectively), even when the SSZ-62 material shows a remarkably lower crystal size (~30-40 nm, see Table 1).

A plausible explanation for the limited catalytic activity of the SSZ-62 zeolite compared to the other nanocrystalline CHA_4 and CHA_5 zeolites, could be found in the lower Si/Al molar ratio of the former. Considering that the theoretical Si/Al molar ratio to ideally obtain one Al per CHA cavity is 11, the preparation of a nanosized CHA zeolite with a lower Si/Al ratio would necessarily result in a material containing more than one Al per cavity, which would accelerate the undesired olefin oligomerization and condensation reactions leading to coke formation and catalyst deactivation. Moreover, it could also be speculated that the formation of bulky aromatic

hydrocarbon pool intermediates in all (or most) of the CHA cavities (see Figure 2a), would result in more diffusional problems for reactant and products, enforcing the catalyst deactivation by coke formation. Thus, it seems that intermediate Si/Al molar ratios (i.e. ~15) would prevent both the diffusional problems offered by the excessive hydrocarbon pool formation within CHA crystals with relatively low Si/Al molar ratios (i.e. ~8), and the moderately catalyst deactivation when only few CHA-cavities are able to induce the hydrocarbon pool formation in zeolites with high Si/Al molar ratios (i.e. ~25).

The results achieved put in relevance how the fine-tune control of the physico-chemical properties of the desired zeolite during its synthesis, undoubtedly allows maximizing the catalyst behavior, particularly for chemical processes with very complex reaction mechanisms, as it is the case of the MTO process. The rationalization of the synthesis of the nanosized CHA zeolite with an optimized aluminum distribution has permitted an outstanding enhancement of its catalytic performance for the MTO reaction.

Acknowledgements

This work has been supported by the European Union through ERC-AdG-2014-671093 (SynCatMatch), by the Spanish Government-MINECO through ‘‘Severo Ochoa” (SEV-2016-0683) and MAT2015-71261-R, and by the Fundación Ramón Areces through a research contract of the “Life and Materials Science” program. E.M.G. acknowledges “La Caixa - Severo Ochoa” International PhD Fellowships (call 2015), C.L. acknowledges China Scholarship Council (CSC) for a Ph.D fellowship, and N.M. thanks MINECO for economical support through a pre-doctoral fellowship (BES-2013-064347). The Electron Microscopy Service of the UPV is acknowledged for their help in sample characterization. Red Española de Supercomputación (RES) and Centre de Càlcul de la Universitat de Valencia are gratefully acknowledged for computational resources and technical support.

Figure 1. Proposed mechanism for the MTO reaction, showing the hydrocarbon pool (HP) species within the CHA cavity, and for catalyst deactivation by formation of polyaromatics

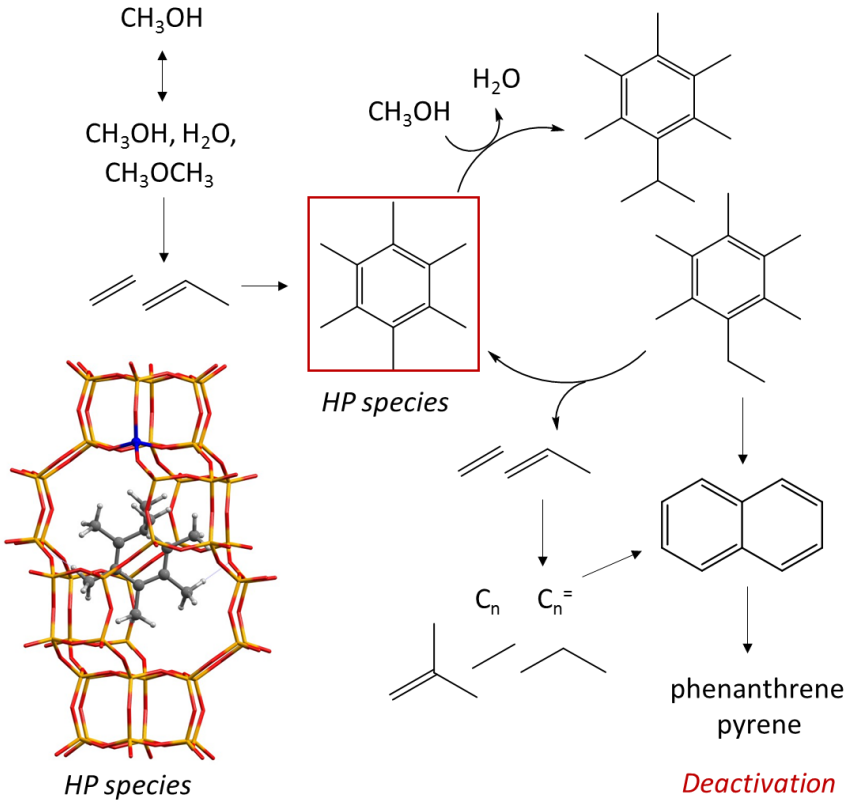

Figure 2. Influence of Al content and distribution on the number of cavities in the CHA structure containing aromatic hydrocarbon pool species. The models correspond to SSZ-13 zeolite with a) Si/Al = 11, b) Si/Al = 15, c) Si/Al = 23 and d) Si/Al = 15 with Al pairs.

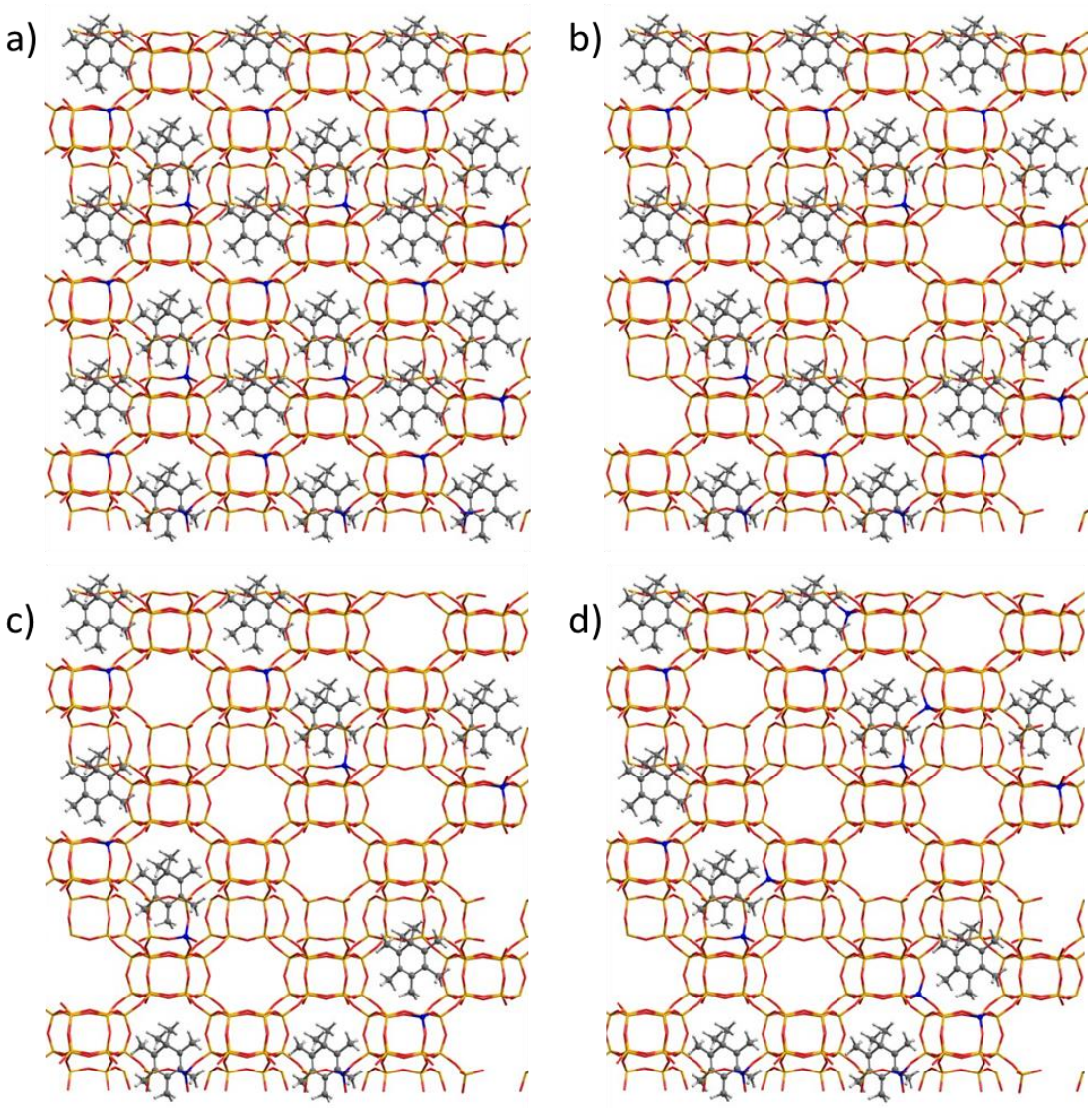

Figure 3: SEM images of the synthesized CHA-related materials

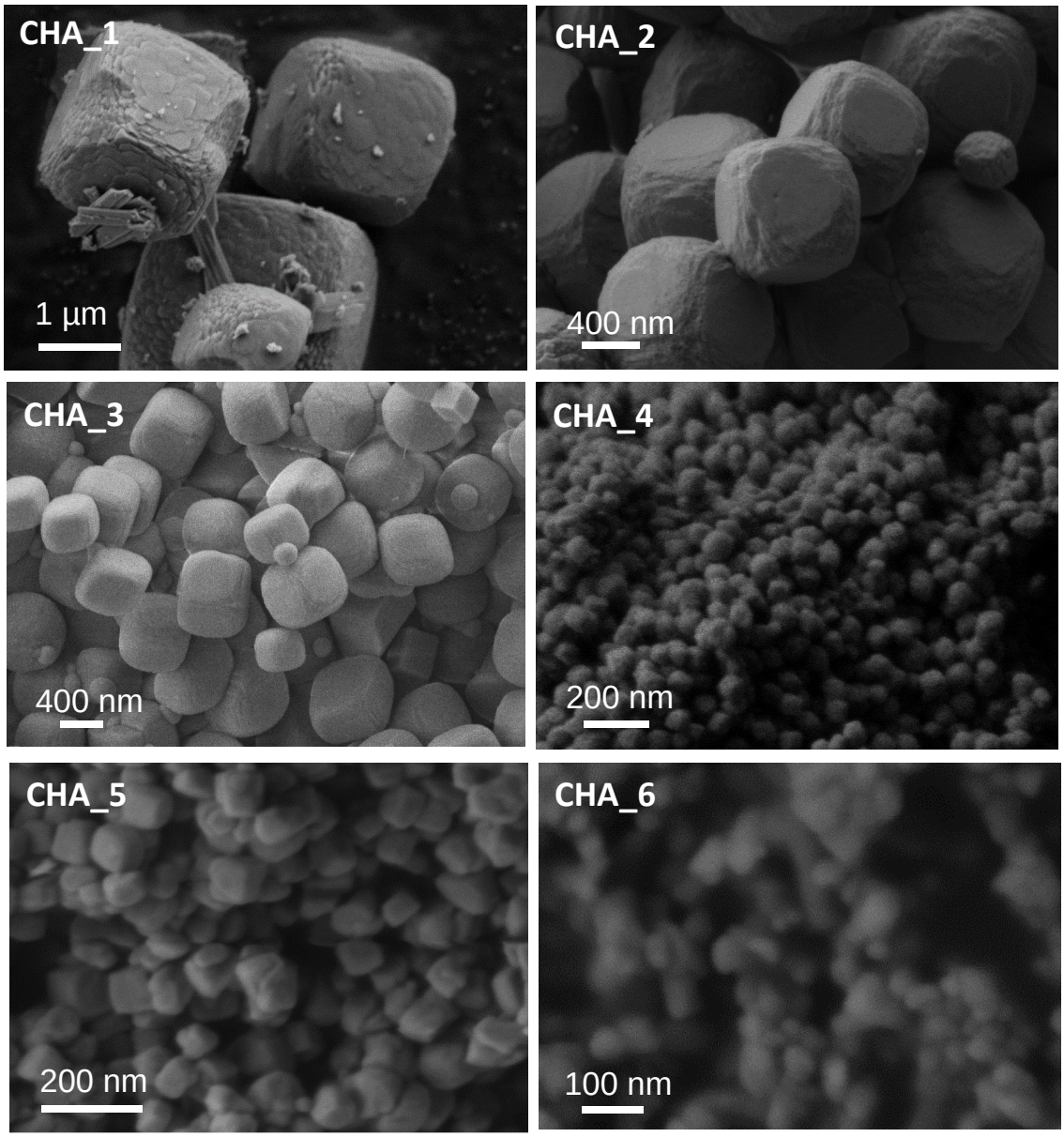

Figure 4: Methanol conversion profiles for the different CHA-related materials. The reaction conditions were: T=350°C, 30 ml/min of N_2 bubbled at -17ºC, WHSV=0.8h^{-1}, W_{cat}=50 mg.

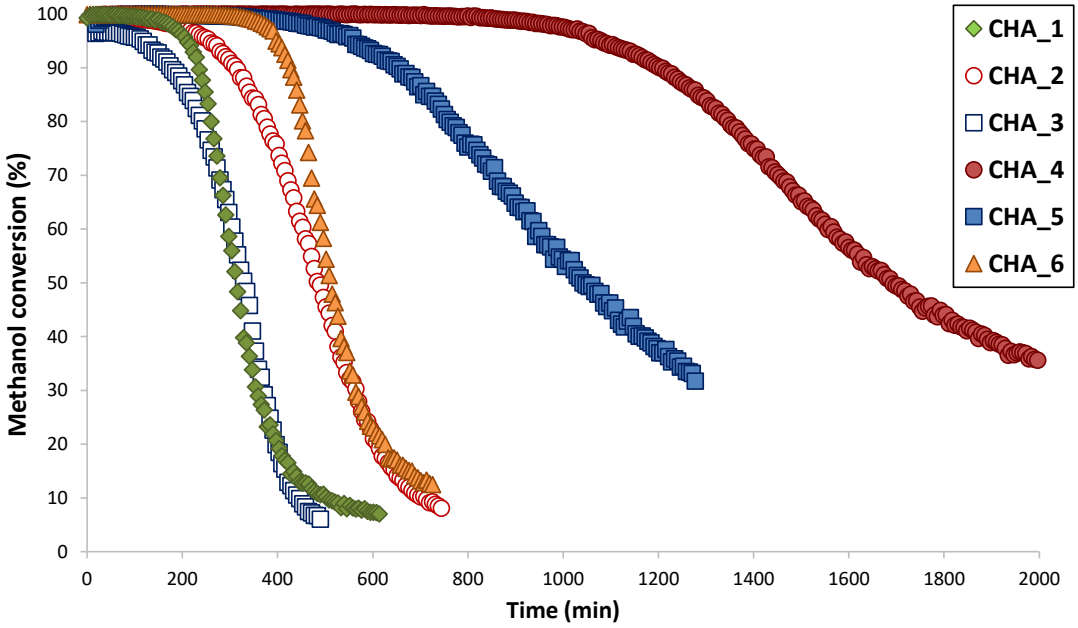

Table 1: Physico-chemical properties of the CHA-related materials in their acid form

Sample	Si/Al	Crystal size (µm)	BET (m^2/g)	S_{micro} (m^2/g)	S_{ext} (m^2/g)	V_{micro} (cm^3/g)
CHA_1	14.9	1.00-2.00	520	517	3	0.25
CHA_2	17.4	0.80-1.00	472	448	24	0.26
CHA_3	26.7	0.70-1.00	596	586	10	0.28
CHA_4	14.2	0.05-0.07	577	495	82	0.25
CHA_5	24.1	0.07-0.09	557	480	76	0.25
CHA_6	8.5	0.03-0.04	630	570	60	0.26

Table 2: Catalytic properties for the different CHA-based zeolites for MTO reaction (reaction conditions: T=350°C, WHSV=0.8 h^{-1}, w_{cat}=50 mg)

	Catalyst lifetime (min)		Selectivity (%) at X_{95}		
Sample	**X_{95}[a]**	**X_{50}[b]**	**$C2^{=}$**	**$C3^{=}$**	**$C4^{=}$**
CHA_1	210	316	39.3	37.8	15.4
CHA_2	260	490	45.1	37.0	12.4
CHA_3	117	335	44.1	36.6	13.0
CHA_4	1085	1693	47.1	34.2	12.1
CHA_5	564	1048	46.8	35.1	12.3
CHA_6	397	514	42.3	40.6	11.9

[a] Methanol conversion drop below 95%
[b] Methanol conversion drop below 50%

Supplementary Material

1.- Experimental section

1.1.- Zeolite synthesis

- Synthesis of the N,N,N-trimethyladamantamonium (TMAda) cation

The hydroxide salt of the N,N,N-trimethyladamantamonium (TMAda) cation was prepared according to the procedure described in the literature.[11]

- Synthesis of CHA_1

CHA_1 (conventional SSZ-13) was synthesized with the following gel composition: 1 SiO_2 : 0.033 Al_2O_3 : 0.2 NaOH : 0.2 TMAdaOH : 44 H_2O, according to the synthesis methodology described in the literature.[9c, 11]

The catalyst was calcined in air at 580°C to remove the template. The acid form of the CHA_1 zeolite was obtained by ion exchange of calcined sample with 2.5 M NH_4Cl solution (80°C and liquid to solid ratio of 10) for 2 hours. Finally, the NH_4-exchanged material was calcined at 500 °C for three hours in air.

- Synthesis of CHA_2

CHA_2 was synthesized with the following gel composition: 1 SiO_2 : 0.033 Al_2O_3 : 0.4 TMAdaOH : 5 H_2O. Aluminum hydroxide (Sigma-Aldrich) was first dissolved in an aqueous solution of TMAdaOH. Then, an amorphous silica (Aerosil) was added, and the resultant mixture gel was allowed to reach the desired silica to water ratio by evaporation under stirring. The gel was transferred into a Teflon-lined steel autoclave and kept statically in an oven at 175°C for 14 days. The product was separated by filtration, washed with deionized water and dried at 100°C. The catalyst was calcined in air at 580°C to remove the template.

- Synthesis of CHA_3

CHA_3 was synthesized with the following gel composition: 1 SiO_2 : 0.016 Al_2O_3 : 0.4 TMAdaOH : 5 H_2O. Aluminum hydroxide (Sigma-Aldrich) was first dissolved in an aqueous solution of TMAdaOH. Then, an amorphous silica (Aerosil) was added, and the resultant mixture gel was allowed to reach the desired silica to water ratio by evaporation under stirring. The gel was transferred into a Teflon-lined steel autoclave and kept statically in an oven at 175°C for 14 days.

The product was separated by filtration, washed with deionized water and dried at 100°C. The catalyst was calcined in air at 580°C to remove the template.

- Synthesis of CHA_4

CHA_4 was synthesized with the following gel composition: 1 SiO_2 : 0.036 Al_2O_3 : 0.4 TMAdaOH : 5 H_2O. The mixture of the commercially available FAU (CBV720, Si/Al~14, Zeolyst, XXXXXXXX) and the aqueous solution of TMAdaOH is maintaining under stirring until the desired silica to water ratio is reached by evaporation. The gel was transferred into a Teflon-lined steel autoclave and kept statically in an oven at 175°C for 14 days. The product was separated by filtration, washed with deionized water and dried at 100°C. The catalyst was calcined in air at 580°C to remove the template.

- Synthesis of CHA_5

CHA_5 was synthesized with the following gel composition: 1 SiO_2 : 0.019 Al_2O_3 : 0.4 TMAdaOH : 5 H_2O. The mixture of the commercially available FAU (CBV760, Si/Al~26, P.Q. Industries, XXXXXXXX) and the aqueous solution of TMAdaOH is maintaining under stirring until the desired silica to water ratio is reached by evaporation. The gel was transferred into a Teflon-lined steel autoclave and kept statically in an oven at 175°C for 14 days. The product was separated by filtration, washed with deionized water and dried at 100°C. The catalyst was calcined in air at 580°C to remove the template.

- Synthesis of CHA_6

CHA_6 was synthesized with the following gel composition: 1 SiO_2 : 0.033 Al_2O_3 : 0.4 NaOH : 0.2 TMAdaOH : 20 H_2O, according to the synthesis methodology described in the literature.[8a] The aqueous solution of TMAdaOH was firstly mixed with NaOH (Sigma-Aldrich), and the required amount of deionized water. Then, aluminum hydroxide (Sigma-Aldrich) was added to the solution mentioned above, and the resulting gel was stirred at 80ºC for 30 minutes. Finally, an aqueous colloidal suspension of an amorphous silica (Ludox, 40%wt., Sigma Aldrich) was added to the gel, and the mixture was stirred at 80ºC for 30 minutes. The resultant gel was transferred into a Teflon-lined steel autoclave in an oven at 160°C for 2 days in static conditions. The product was separated by filtration, washed with deionized water and dried at 100°C. The catalyst was calcined in air at 580°C to remove the template. The acid form of the CHA_6 material was obtained by ion exchange of the calcined sample with 1 M NH_4Cl solution for 2 hours (80°C and liquid to solid ratio of 10), and a calcination treatment at 500 °C for three hours in air.

2.2.- Characterization

The crystallization of the samples was studied by powder X-ray diffraction (PXRD) using a Panalytical CUBIX diffractometer with monochromatic $CuK_{\alpha 1,2}$ radiation (λ=1.5406, 1.5444 Å; $K\alpha_2/K\alpha_1$ intensity ratio=0.5).

The morphology and particle size of the zeolites were characterized by Scanning Electron Microscope (SEM, JEOL JSM-6300).

The solid MAS NMR spectra were recorded with a Bruker AV400 spectrometer. Solid state ^{27}Al MAS NMR spectra were recorded at 104.218 MHz with a spinning rate of 10 kHz at a 90º pulse length of 0.5 μs with 1 s repetition time. The ^{27}Al chemical shift was referred to $Al(H_2O)_6$.

The chemical composition of the solid samples was determined by inductively coupled plasma atomic absorption spectroscopy (ICP-OES) using a Varian 715-ES.

Textural properties were determined by N_2 adsorption isotherms measured at 77 K with a Micromeritics ASAP 2020.

Cation-exchange of zeolite samples with Co^{2+}: First, the zeolite samples were dried in air at 100°C overnight. Then, a 0.05 M aqueous solution of $Co(NO_3)_2$ was added (liquid : solid = 150 ml/g) and the resultant mixture kept under stirring at room temperature for 24 h. After the cation exchange, the solids were filtered and washed with abundant deionized water. Finally, the Co-exchanged samples were dried in vacuum at room temperature for 16 h to eliminate the physically adsorbed water.

2.3- Computational Details

Periodic density functional calculations were performed using the Perdew-Wang (PW91) exchange-correlation functional within the generalized gradient approach (GGA)[13] as implemented in the VASP code.[14] The valence density was expanded in a plane wave basis set with a kinetic energy cutoff of 450 eV, and the effect of the core electrons in the valence density was taken into account by means of the projected augmented wave (PAW) formalism.[15] Integration in the reciprocal space was carried out at the Γ k-point of the Brillouin zone. Electronic energies were converged to 10^{-6} eV and geometries were optimized until forces on atoms were less than 0.015 eV/Å. During geometry optimizations the positions of all atoms in the system were allowed to relax without any restriction.

The chabazite structure was modelled by means of a hexagonal unit cell with lattice parameters a = b = 13.8026 Å, c = 15.0753 Å, $\alpha = \beta$ = 90º and γ = 120º containing 36 Si and 72 O atoms. To study the preferential location of $TMAada^+$ and Na^+ as compensating cations in relation to Al, (results in Figure S1a,b) only one framework Si atom per unit cell was substituted by Al, generating catalyst models with Si/Al = 35. To study the relative stability of different types of Al

pairs (results in Figure S1c,d) two framework Si atoms per unit cell were replaced by Al, generating catalyst models with Si/Al = 17. Finally, to study the influence of the compensating cation on the global distribution of Al (results in Figure S2 and Table S1), three framework Si per unit cell were substituted by Al generating catalyst models with Si/Al = 11.

The relative stability (E_{rel}) of all structures with the same composition was calculated according to:

$E_{rel} = E_X - E_M$

where E_X and E_M are the total energies of the structure considered (X) and the most stable one (M), respectively.

2.4.- Catalytic experiments

The catalyst was pelletized, crushed and sieved into 0.2-0.4 mm particle size. 50 mg of sample was mixed with 2 g quartz (Fluka) before being introduced into the fixed-bed reactor (7mm diameter). N_2 (30mL/min) was bubbled in methanol hold at -17°C, giving a WHSV=0.8 h^{-1}. The catalyst was first activated with a nitrogen flow of 80 ml/min for 1 h at 540°C, and then the temperature was decreased to reaction conditions (350°C). Each experiment was analyzed every 5 minutes with an online gas chromatograph (Bruker 450GC, with PONA and Al_2O_3-Plot capillary columns, and two FID detectors). After reaction, the catalyst was regenerated at 540°C in 80ml of air for 3h and the reaction was repeated again. Conversion and selectivities were considered in carbon basis and methanol and dimethylether were lumped together for calculation of conversion.

Figure S1: CHA structure containing one Al compensated by a) $TMAda^+$ and b) Na^+ cations. c) Different Al pair distributions and d) an Al pair compensated by $TMAda^+$ + Na^+. Relative energies of different locations of compensating cations are given in kcal/mol. The regular and bold values in c) correspond to $2TMAda^+$ and $TMAda^+$+Na^+ compensating the two Al, respectively.

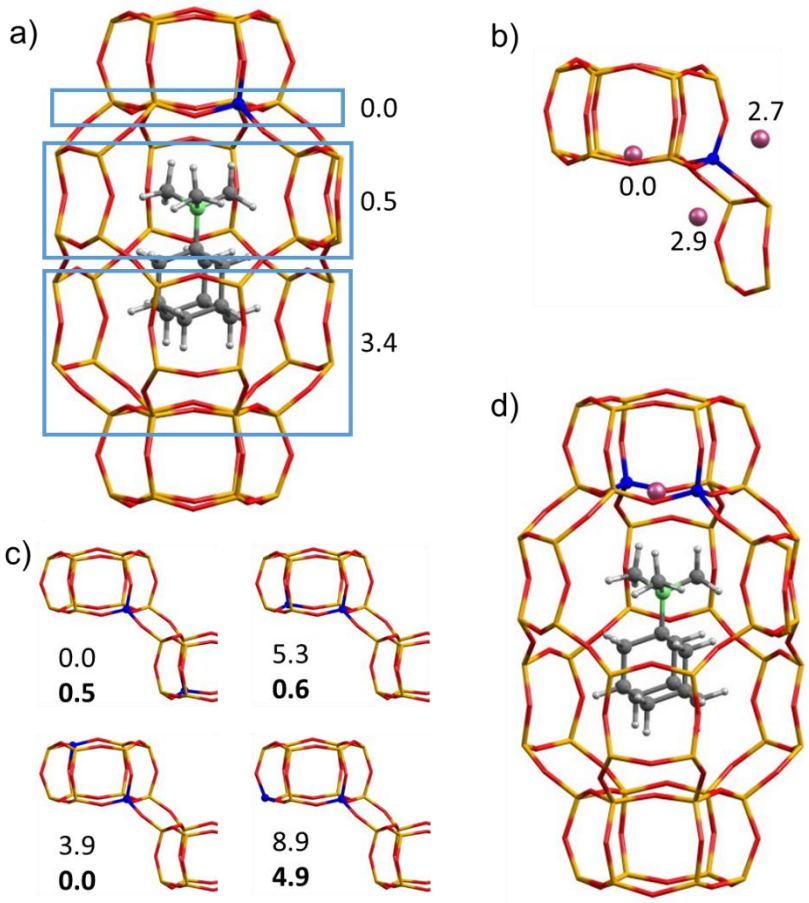

Figure S2: Al distributions in SSZ-13 with Si/Al = 11 summarized in Table S1.

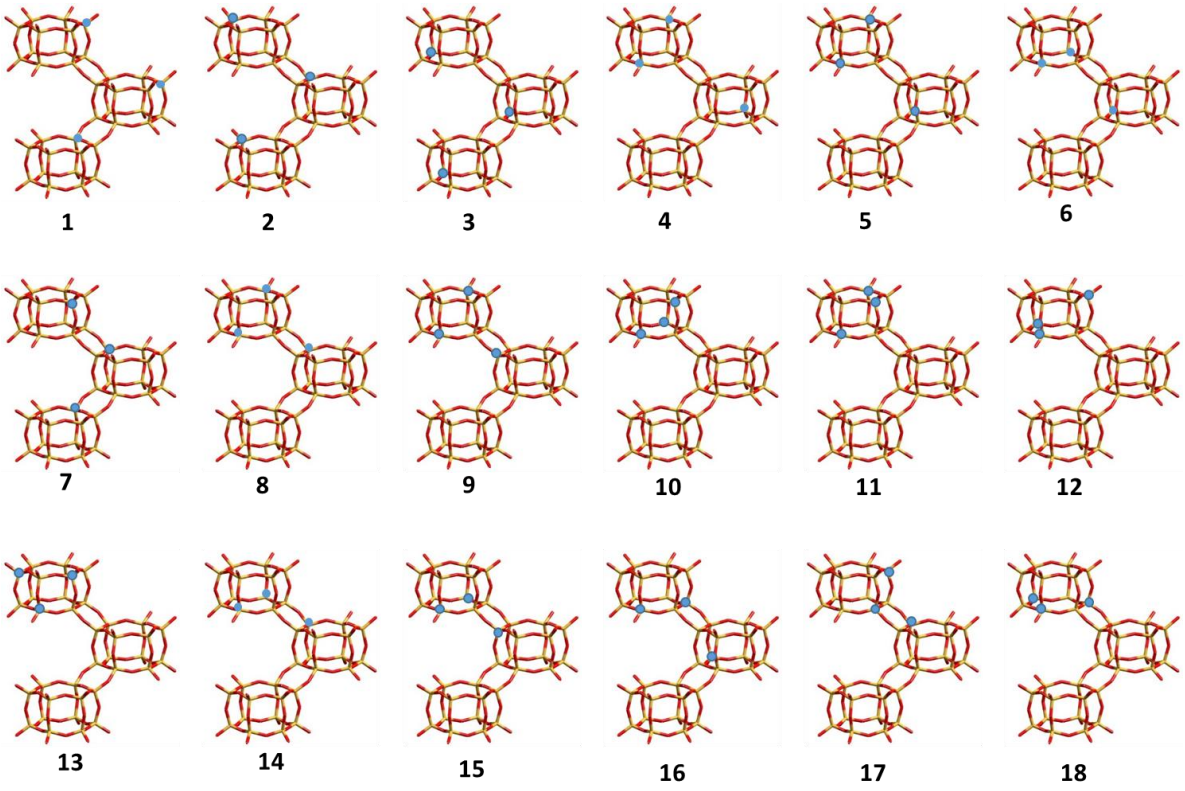

Figure S3: PXRD patterns of the as-prepared CHA-related materials

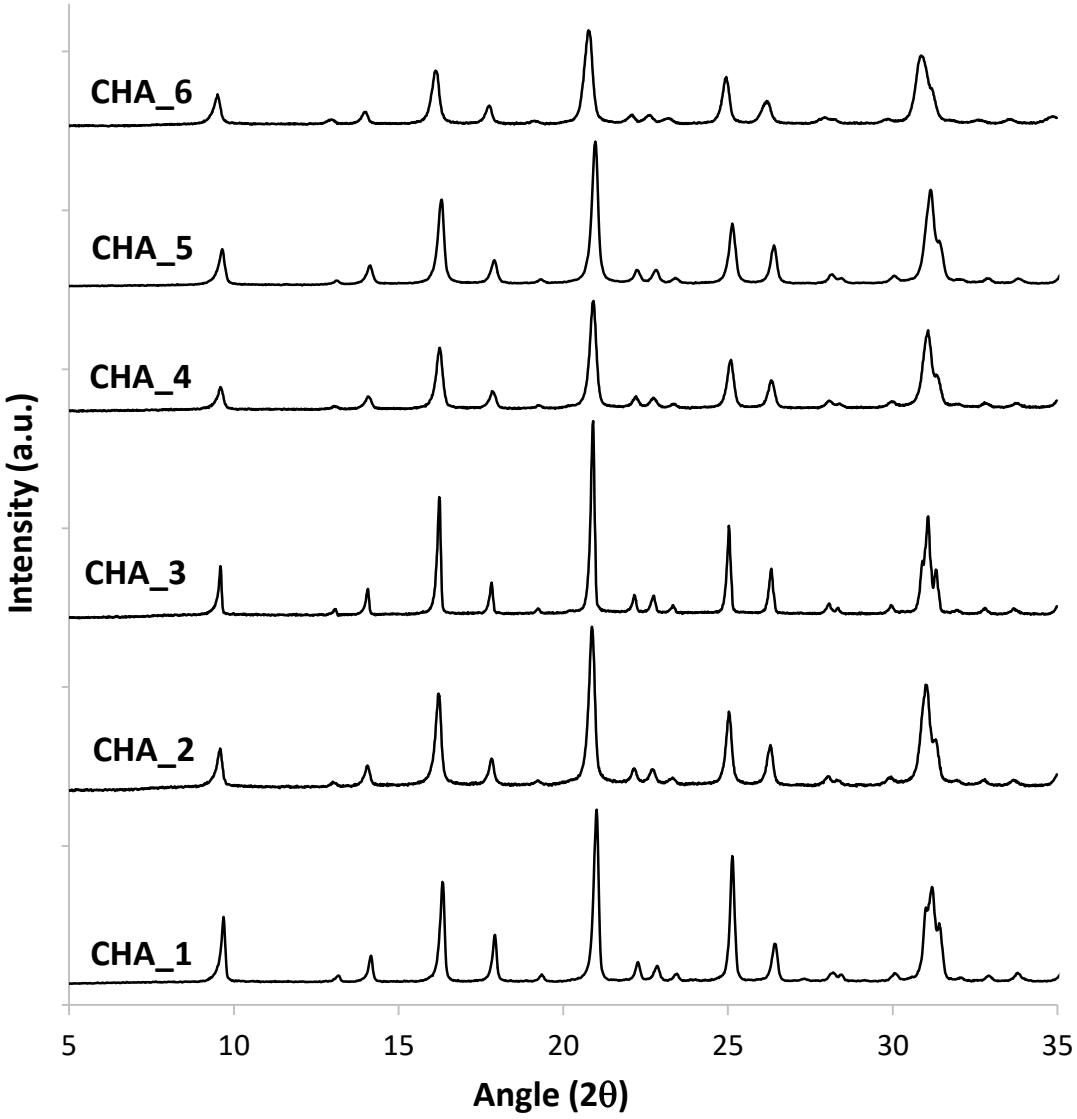

Figure S4: ^{27}Al MAS NMR spectra of the CHA-related materials after being calcined and NH_4^+-exchanged

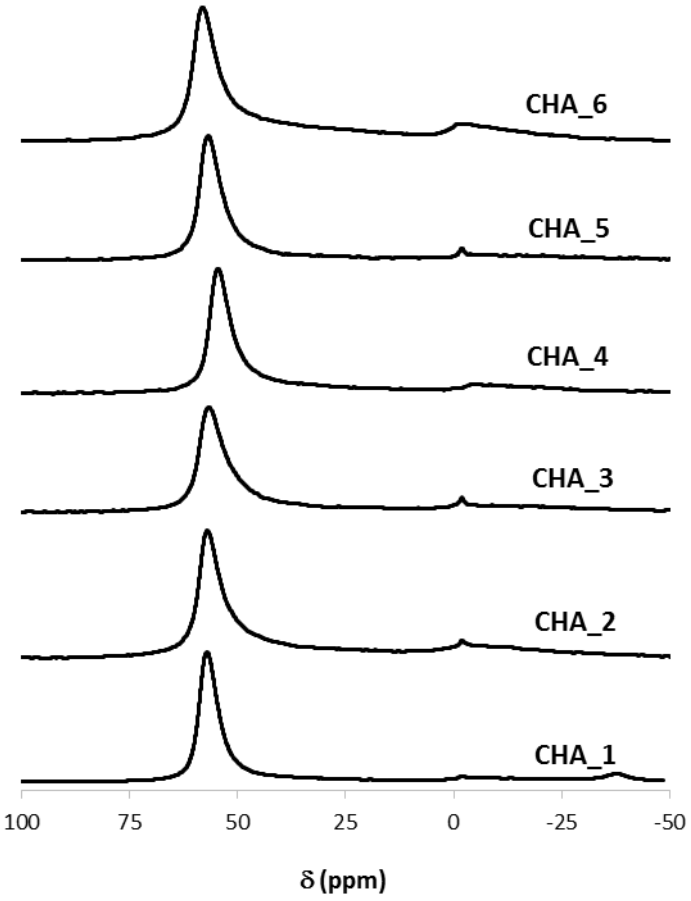

Figure S5: Methanol conversion (a) and product selectivities (b) achieved using the CHA_1 zeolite as catalyst for the MTO reaction (reaction conditions: T=350°C, WHSV=0.8 h^{-1}, w_{cat}=50 mg)

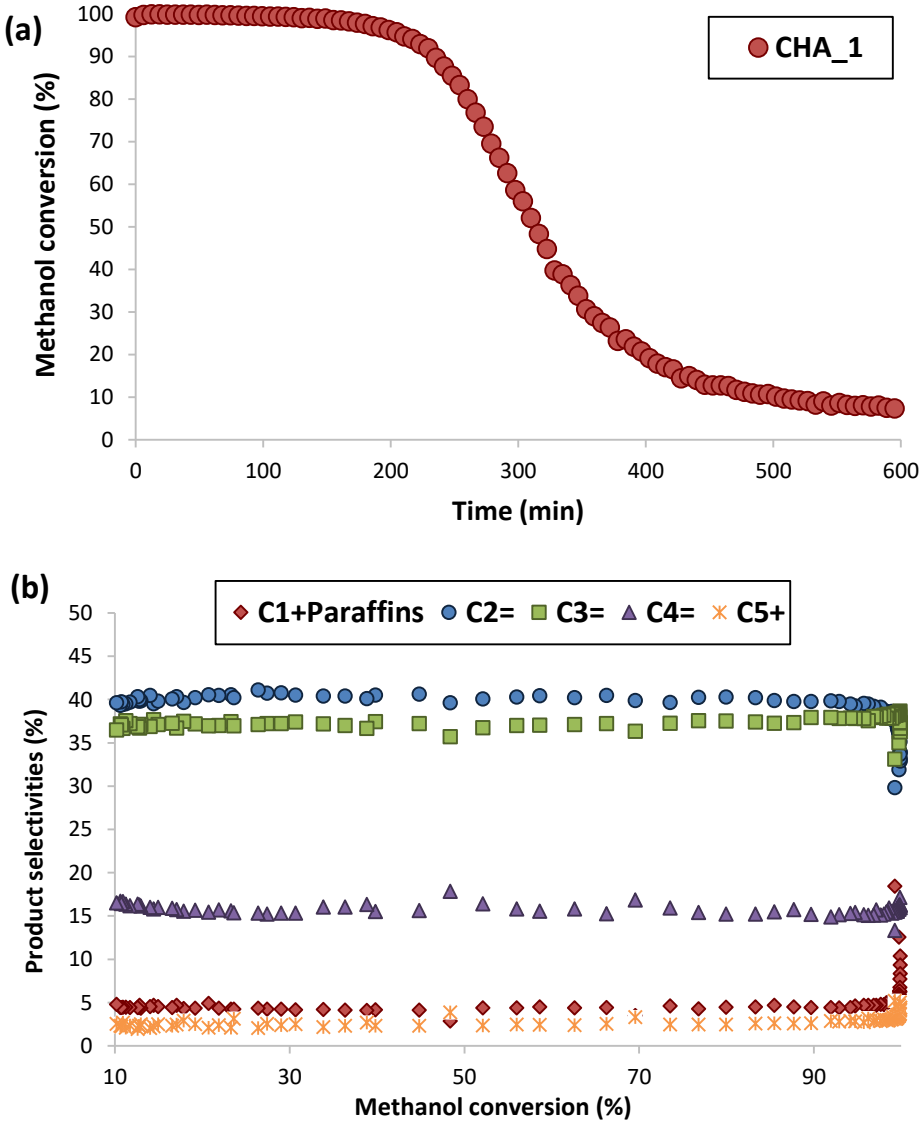

Figure S6: Methanol conversion (a) and product selectivities (b) achieved using the CHA_2 zeolite as catalyst for the MTO reaction (reaction conditions: T=350°C, WHSV=0.8 h^{-1}, w_{cat}=50 mg)

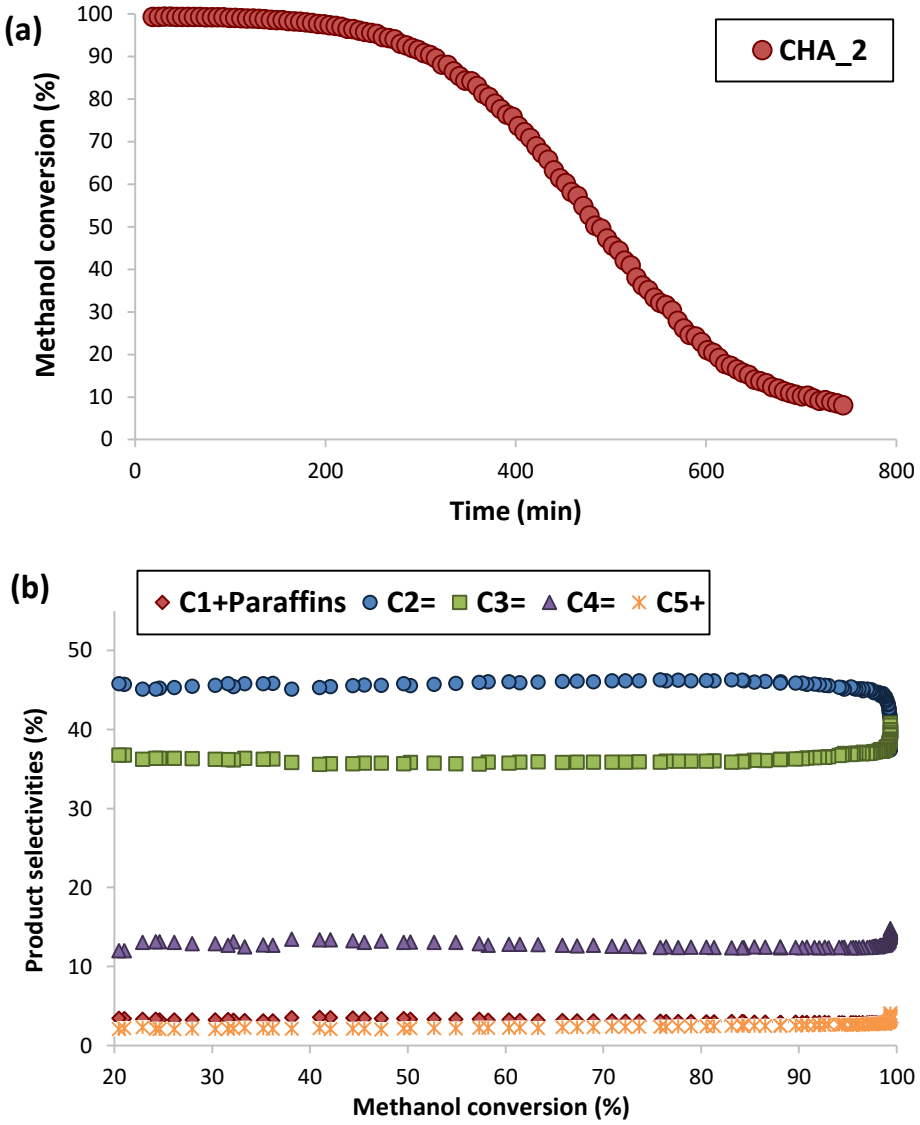

Figure S7: Methanol conversion (a) and product selectivities (b) achieved using the CHA_3 zeolite as catalyst for the MTO reaction (reaction conditions: T=350°C, WHSV=0.8 h^{-1}, w_{cat}=50 mg)

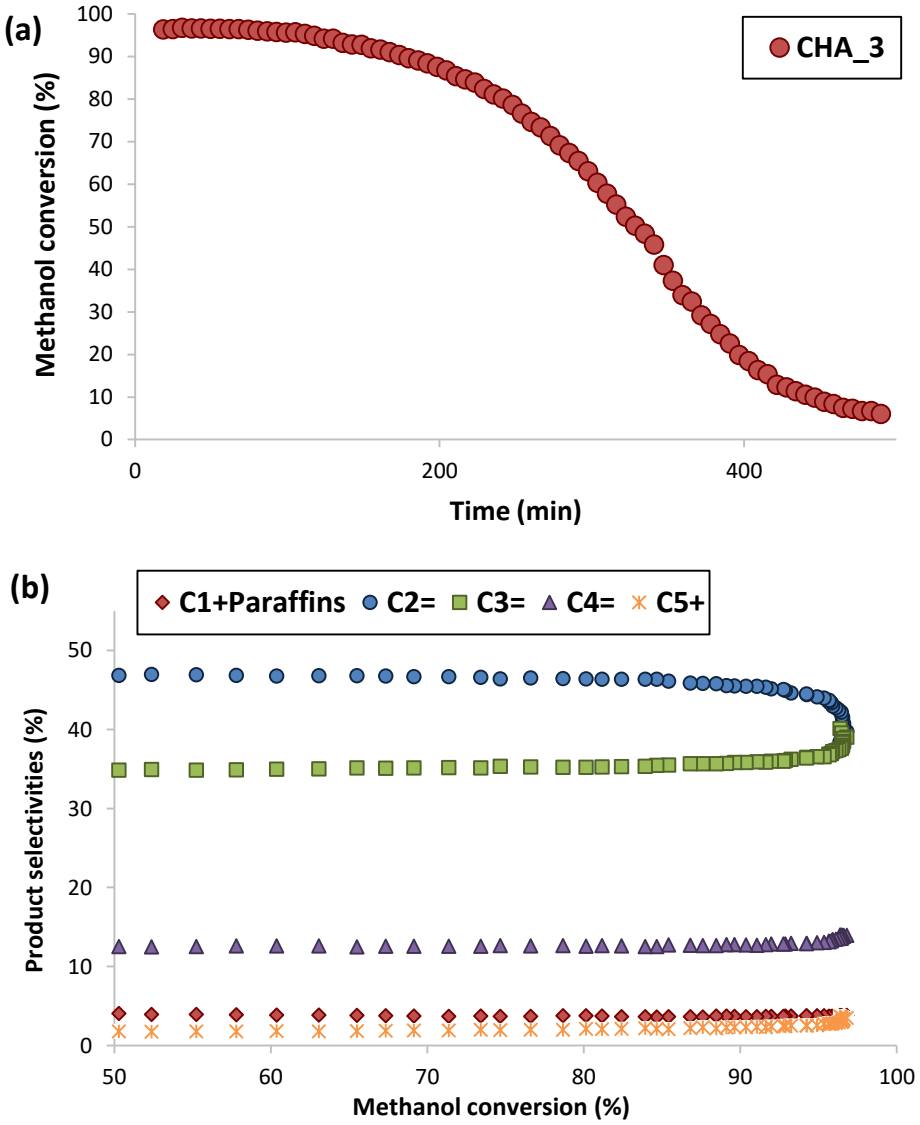

Figure S8: Methanol conversion (a) and product selectivities (b) achieved using the CHA_4 zeolite as catalyst for the MTO reaction (reaction conditions: T=350°C, WHSV=0.8 h^{-1}, w_{cat}=50 mg)

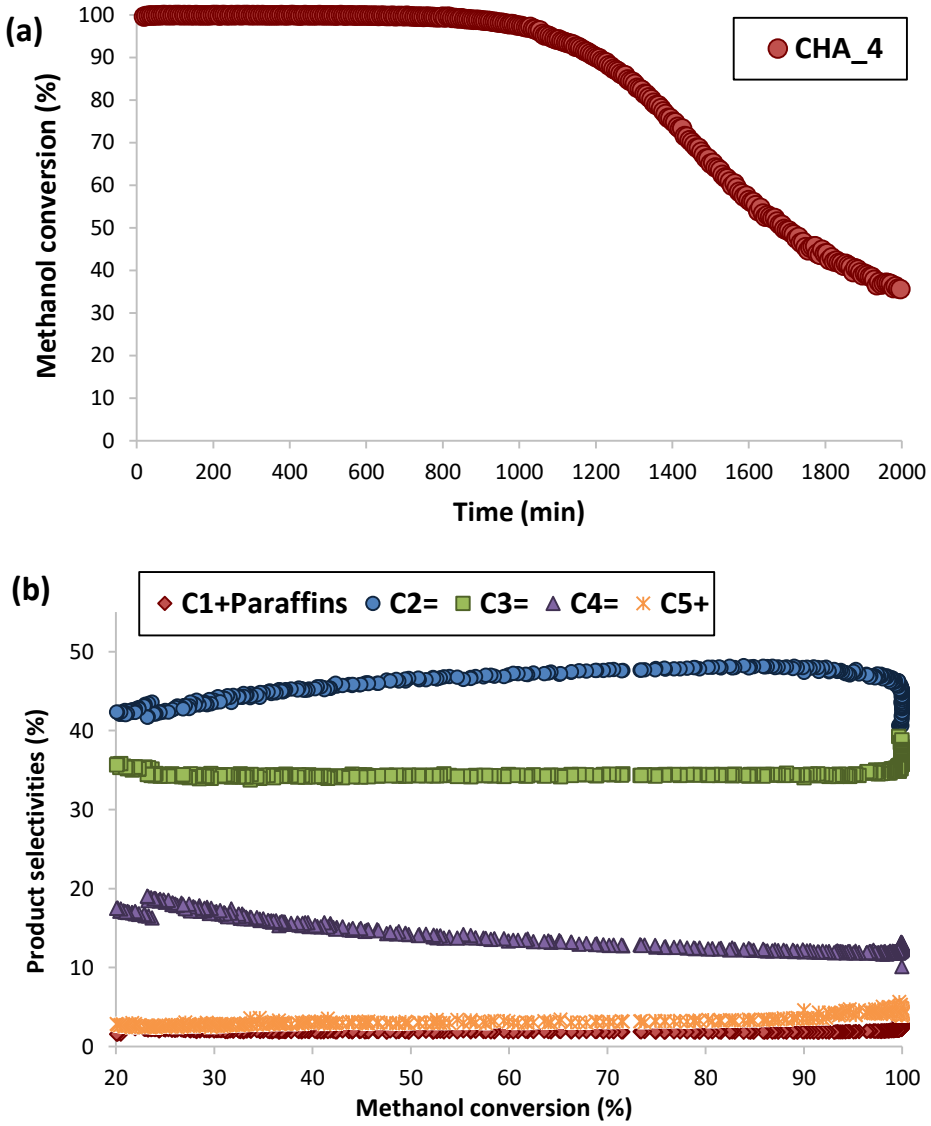

Figure S9: Methanol conversion (a) and product selectivities (b) achieved using the CHA_5 zeolite as catalyst for the MTO reaction (reaction conditions: T=350°C, WHSV=0.8 h^{-1}, w_{cat}=50 mg)

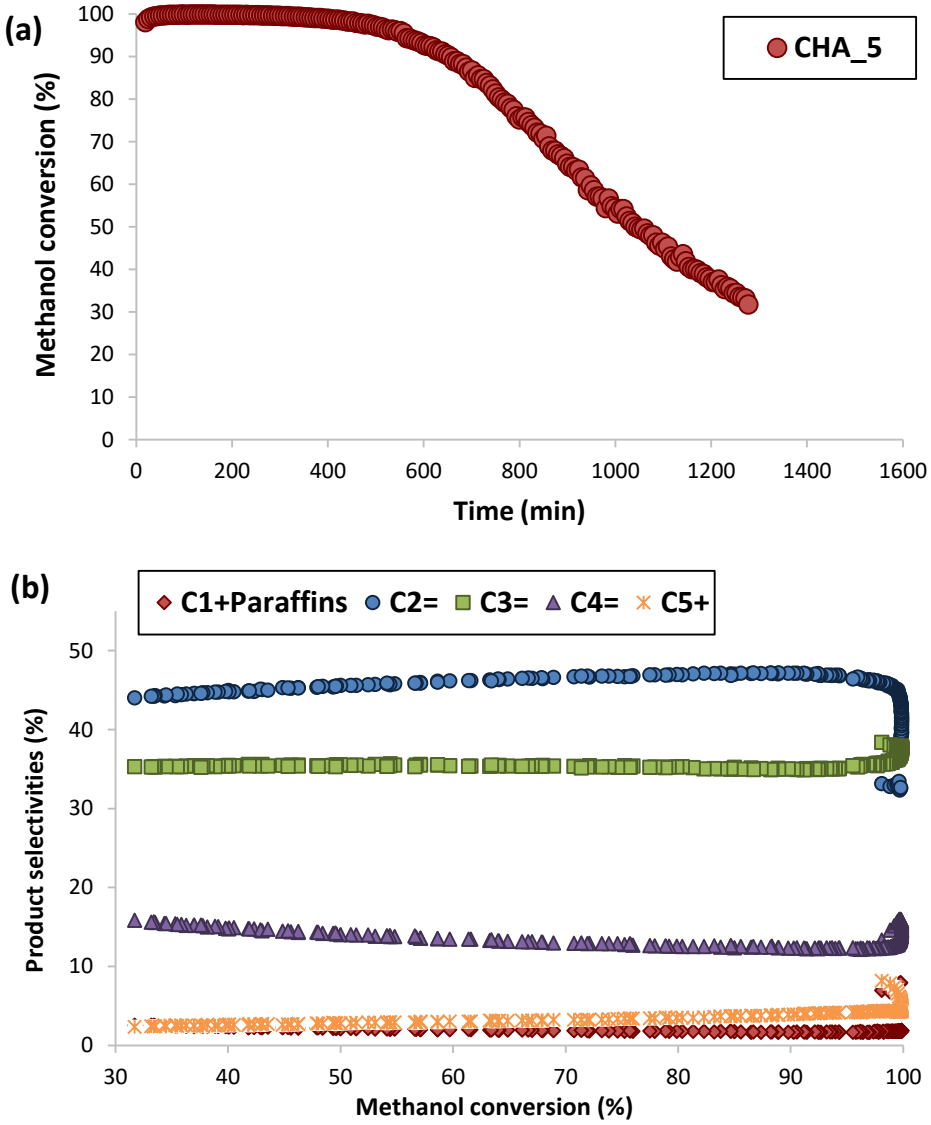

Figure S10: Methanol conversion (a) and product selectivities (b) achieved using the CHA_6 zeolite as catalyst for the MTO reaction (reaction conditions: T=350°C, WHSV=0.8 h^{-1}, w_{cat}=50 mg)

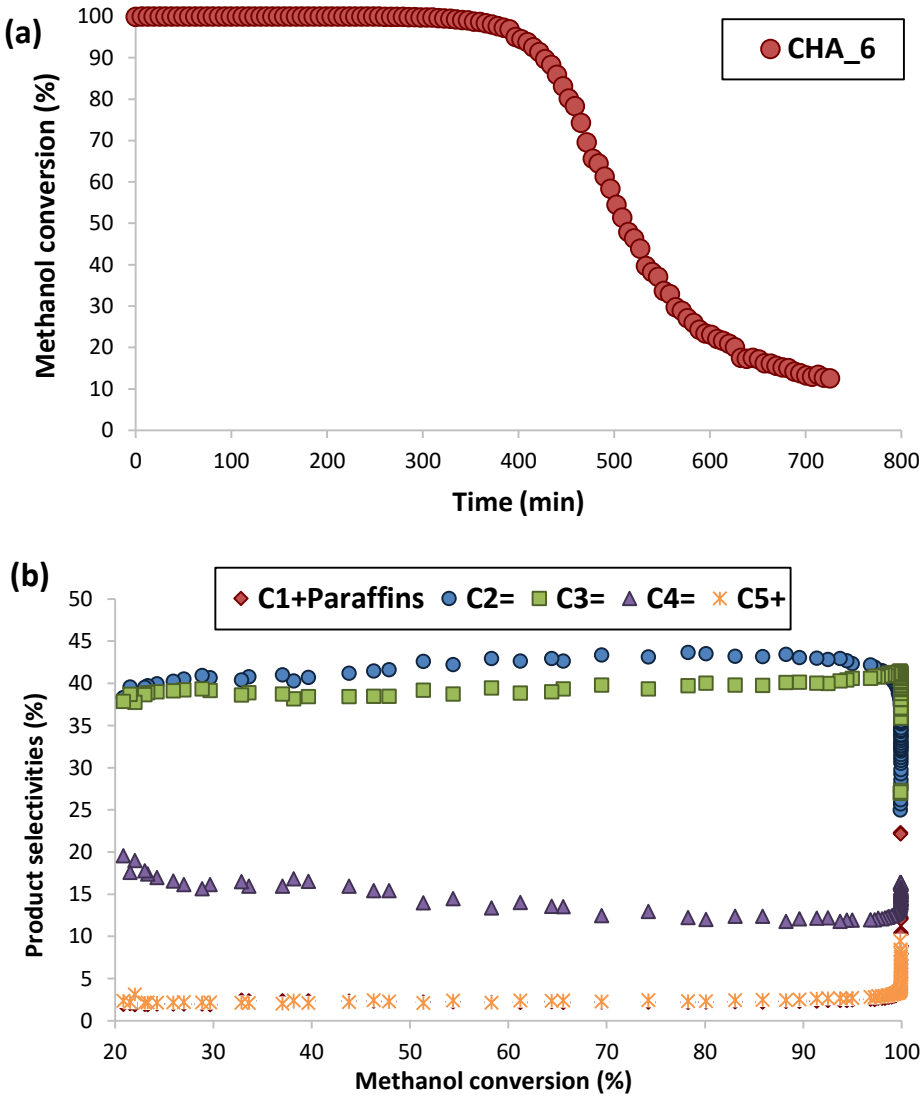

Table S1: Relative stability (in kcal/mol) of different distributions of Al in SSZ-13 depending on the SDA compensating cation.

	Number of Al atoms in the same:				Al-pairs		Relative stability (kcal/mol)	
	cavity	D6R	8R	6R	x=1	x=2	TMAda+	$TMAda^{+}+Na^{+}$
1	1	1	1	1	0	0	0.0	3.4
2	1	1	1	1	0	0	3.6	6.4
3	1	1	1	1	0	0	2.0	2.6
4	1	2	1	1	0	0	0.9	1.2
5	1	2	1	1	0	0	0.9	0.6
6	2	2	1	2	0	1	1.4	0.0
7	2	1	1	1	0	2	9.4	10.1
8	2	2	1	1	0	2	6.9	7.8
9	2	2	2	1	1	0	8.5	9.1
10	2	3	1	2	1	2	12.6	4.3
11	2	3	1	2	2	0	14.7	5.0
12	2	3	1	2	1	2	10.9	8.6
13	2	3	1	2	3	0	21.7	11.6
14	3	2	1	2	1	1	15.5	7.3
15	3	2	2	2	1	1	12.0	7.9
16	3	2	2	2	2	0	9.7	9.7
17	3	2	1	1	3	0	20.4	20.2
18	3	3	1	3	3	0	15.6	8.0

Table S2: Synthesis conditions

Sample	Si source / Al source	Si/Al	NaOH/Si	OSDA
CHA_1	SiO_2 / $Al(OH)_3$	15	0.2	TMAda
CHA_2	SiO_2 / $Al(OH)_3$	15	0.0	TMAda
CHA_3	SiO_2 / $Al(OH)_3$	25	0.0	TMAda
CHA_4	FAU (CBV720)	14	0.0	TMAda
CHA_5	FAU (CBV760)	26	0.0	TMAda
CHA_6	SiO_2 / $Al(OH)_3$	15	0.4	TMAda

Table S3: Amount of aluminum-pairs calculated after Co-exchange treatments, and chemical composition on the external surface of the crystals measured by XPS

Sample	Si/Al	Co/Al	Al_{pair} (%)
CHA_1	14.9	0.055	10.9
CHA_2	17.4	0.024	4.8
CHA_3	26.7	0.022	4.4

References:

[1] P. Tian, Y. Wei, M. Ye, Z. Liu, *ACS Catal.* **2015**, *5*, 1922-1938.

[2] (a) U. Olsbye, S. Svelle, M. Bjørgen, P. Beato, T. V. W. Janssens, F. Joensen, S. Bordiga, K. P. Lillerud, *Angew. Chem., Int. Ed.* **2012**, *51*, 5810-5831; (b) M. Moliner, C. Martínez, A. Corma, *Chem. Mater.* **2014**, *26*, 246-258.

[3] M. Stöcker, *Micropor. Mesopor. Mater.* **1999**, *29*, 3-48.

[4] (a) S. Wilson, P. Barger, *Micropor. Mesopor. Mater.* **1999**, *29*, 117-126; (b) K. Hemelsoet, J. Van der Mynsbrugge, K. De Wispelaere, M. Waroquier, V. S. V., *ChemPhysChem* **2013**, *14*, 1526-1545.

[5] (a) J. F. Haw, D. M. Marcus, *Top. Catal.* **2005**, *34*, 41-48; (b) F. Bleken, M. Bjørgen, L. Palumbo, S. Bordiga, S. Svelle, K. P. Lillerud, U. Olsbye, *Top. Catal.* **2009**, *52*, 218–228.

[6] B. M. Lok, C. A. Messina, R. L. Patton, R. T. Gajek, T. R. Cannan, E. M. Flanigen, *J. Am. Chem. Soc.* **1984**, *106*, 6092-6093.

[7] J. Q. Chen, A. Bozzano, B. Glover, T. Fuglerud, S. Kvisle, *Catal. Today* **2005**, *106*, 103-107.

[8] (a) S. I. Zones, L. T. Yuen, S. J. Miller, *WO/2003/020641* **2003**; (b) T. Takata, N. Tsunoji, Y. Takamitsu, M. Sadakane, T. Sano, *Microp. Mesop. Mater.* **2016**, *225*, 524-533.

[9] (a) L. Wu, V. Degirmenci, P. C. M. M. Magusin, B. M. Szyja, E. J. M. Hensen, *Chem. Commun.* **2012**, *48*, 9492-9494; (b) L. Wu, V. Degirmenci, P. C. M. M. Magusin, N. J. H. G. M. Lousberg, E. J. M. Hensen, *J. Catal.* **2013**, *298*, 27-40; (c) Z. Li, M. T. Navarro, J. Martinez-Triguero, J. Yu, A. Corma, *Catal. Sci. Technol.* **2016**, *6* 5856-5863; (d) X. Zhu, N. Kosinov, J. P. Hofmann, B. Mezari, Q. Qian, R. Rohling, B. M. Weckhuysen, J. Ruiz-Martínez, E. J. M. Hensen, *Chem. Commun.* **2016**, *52*, 3227-3230.

[10] J. R. Di Iorio, R. Gounder, *Chem. Mater.* **2016**, *28*, 2236-2247.

[11] S. I. Zones, *US4544538* **1985**.

[12] (a) N. Martin, Z. Li, J. Martinez-Triguero, J. Yu, M. Moliner, A. Corma, *Chem. Commun.* **2016**, *52*, 6072-6075; (b) D. Xie, S. I. Zones, R. J. Saxton, *WO2016/032565* **2016**.

[13] (a) J. P. Perdew, J. A. Chevary, S. H. Vosko, K. A. Jackson, M. R. Pederson, D. J. Singh, C. Fiolhais, *Phys. Rev. B* **1992**, *46*, 6671-6687; (b) J. P. Perdew, Y. Wang, *Phys. Rev. B* **1992**, *45*, 13244-13249.

[14] (a) G. Kresse, J. Furthmüller, *Phys. Rev. B* **1996**, *54*, 11169-11186; (b) G. Kresse, J. Hafner, *Phys. Rev. B* **1993**, *47*, 558-561.

[15] P. E. Blöchl, *Phys. Rev. B 1994, 50* **1994**, *50*, 17953-17979.